



# CHEM MED CHEM

CHEMISTRY ENABLING DRUG DISCOVERY

## Accepted Article

**Title:** Design, Synthesis and Biological Evaluation of New Type II B-RafV600E Inhibitors

**Authors:** Peng-Fei Wang, Ze-Feng Wang, Han-Yue Qiu, Yue Huang, Hui-Min Hu, Zhong-Chang Wang, and Hai-Liang Zhu

This manuscript has been accepted after peer review and appears as an Accepted Article online prior to editing, proofing, and formal publication of the final Version of Record (VoR). This work is currently citable by using the Digital Object Identifier (DOI) given below. The VoR will be published online in Early View as soon as possible and may be different to this Accepted Article as a result of editing. Readers should obtain the VoR from the journal website shown below when it is published to ensure accuracy of information. The authors are responsible for the content of this Accepted Article.

**To be cited as:** *ChemMedChem* 10.1002/cmdc.201800574

**Link to VoR:** <http://dx.doi.org/10.1002/cmdc.201800574>

WILEY-VCH

[www.chemmedchem.org](http://www.chemmedchem.org)

A Journal of



## FULL PAPER

# Identification and Biological Evaluation of New Type II B-Raf<sup>V600E</sup> Inhibitors

Peng-Fei Wang,<sup>†[a]</sup> Ze-Feng Wang,<sup>†[a]</sup> Han-Yue Qiu,<sup>[a]</sup> Yue Huang,<sup>[b]</sup> Hui-Min Hu,<sup>[a]</sup> Zhong-Chang Wang,<sup>\*[a]</sup> and Hai-Liang Zhu<sup>\*[a]</sup>

[a] Dr. Peng-Fei Wang; Ze-Feng Wang; Dr. Han-Yue Qiu; Hui-Ming Hu; Dr. Zhong-Chang Wang; Prof. Hai-Liang Zhu, State Key Laboratory of Pharmaceutical Biotechnology, Nanjing University, Nanjing 210023, People's Republic of China  
E-mail: zhuhl@nju.edu.cn

[b] Dr. Yue Huang, College of Light Industry and Food Engineering, Nanjing Forestry University, Nanjing 210037, People's Republic of China

<sup>†</sup>These two authors contributed equally to this paper.

Supporting information for this article is given via a link at the end of the document.

**Abstract:** The MAPK (Mitogen-activated protein kinase) pathway plays a vital role in the signal transduction network. Severe diseases may be triggered when it is disturbed by mutated components especially the B-Raf<sup>V600E</sup> kinase. New agents for the kinase are ever needed as cases of relapse and resistance for the known drugs have been widely reported in therapy. In the present work, we have identified a new class of B-Raf<sup>V600E</sup> inhibitors by fragment linking. *In vitro* and *in vivo* assays were employed to depict the pharmacological properties of the compounds, which suggest **5v** (3-(3-(4-chloro-3-(trifluoromethyl)phenyl)ureido)-N-(1-(4-methoxyphenyl)-1H-pyrazol-4-yl)benzamide) is the most potent agent with IC<sub>50</sub> values of 0.035 ± 0.004 μm (B-Raf<sup>V600E</sup> kinase) and 0.39 ± 0.04 μm (A375 cells). Meanwhile, no obvious toxicity was observed. Collectively, the results favored our design intention and hinted that this new kind of chemotype may worth further study in developing novel B-Raf candidates.

## Introduction

It has long been a hot topic to explore new chemotypes for B-Raf kinase inhibitors.<sup>[1]</sup> As a key component in the ERK signal pathway, B-Raf kinase cascades the upstream signals transduced from Ras to downstream module MEK.<sup>[2]</sup> This cascade is precisely executed in normal cells, and when morbidly activated by mutated B-Raf kinase (most commonly B-Raf<sup>V600E</sup>), severe diseases including malignant tumors could be triggered.<sup>[3]</sup> Several agents targeting the hyperactive Raf kinase have been approved into the market, and more types of potential inhibitors are in the evaluation stage.<sup>[4]</sup> However, the pharmaceutical market still calls for new and safe medicines as there remain nonnegligible drawbacks for the known B-Raf inhibitors.<sup>[5]</sup> Taken vemurafenib as an example, it's the most successful case of employing FBDD (Fragment-Based Drug Design) strategy and proved to be a potent and selective inhibitor for the B-Raf<sup>V600E</sup> mutant kinase.<sup>[6]</sup> Yet it's plagued by the relapse and resistance, along with the side effects.<sup>[7]</sup> In addition, sorafenib and other agents also face the kinase selectivity problems.<sup>[8]</sup>

By far, massive research studies have been carried out to elucidate the underlying mechanisms and to seek for new agents with better performance.<sup>[9]</sup> As a kinase, B-Raf may take on three types of conformation, *i.e.* the type I, type II and type I/II conformation.<sup>[10]</sup> The major differences between those types mainly lay in the back pocket (BP) region, both in the size and number of subpockets.<sup>[11]</sup> While the type I protein has the smallest BP region and type I/II the intermediate, the type II protein contains the largest BP region and concomitantly the most subpockets. On the other side, the front pocket (FP) region for all the types keeps almost the same. Therefore, different types of kinase inhibitors may share similar fragment and interacting mode in the FP region of different conformational proteins.<sup>[12]</sup> Interestingly, type II inhibitors of kinase have the least risk to induce the paradoxical effect in B-Raf<sup>WT</sup> cells (induce the kinase activity in low doses and decrease it in high doses). Developing new type II inhibitors thereby is more likely to bring out paradox breakers.<sup>[13]</sup>

In our previous work, new type I B-Raf<sup>V600E</sup> inhibitors were designed by deconstruction-reconstruction strategy.<sup>[14]</sup> The recombinant molecules have been proved to be potent inhibitors for B-Raf<sup>V600E</sup> kinase and the *in silico* model helped to reveal the putative binding mode. It is of interest to note that despite the structural diversity, our molecules share a similar hydrogen-bonding mode with the typical known type II B-Raf inhibitors in the FP pocket region. Thus new hybridized inhibitors might be developed by the recombination of these two types of molecules. As shown in Fig. 1, both the reported molecule and control agent sorafenib hydrogen bond with the key amino residues of the receptor, *i.e.* Cys532 in the hinge region and Asp594 in the DFG motif. In consideration that the diphenylurea is one of the most prevalent scaffolds employed in type II kinase inhibitors which well accommodated in the BP region, it's more guaranteed to start from this backbone for new agent design. Meanwhile, as the type I and type II kinases have different distances between DFG motif to the FP, the recombination needs a suitable linker to bridge the distance gap. Based on this knowledge, we have designed several linkers to accomplish the connection. The new molecules were then investigated by consensus docking to observe whether

## FULL PAPER

the components keep original binding interactions and to rank the binding affinities. The lead compound was validated and further simulated by molecular dynamics before modified and iteratively docked. Afterward, the compounds were synthesized and tested by a series of bioassays to establish pharmacological profiles and a SAR model.

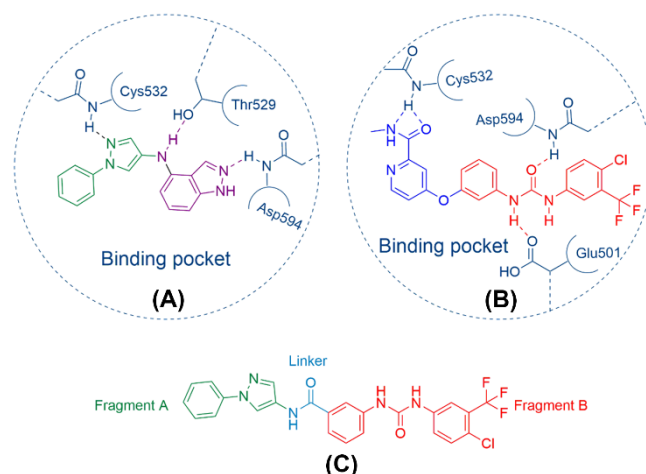


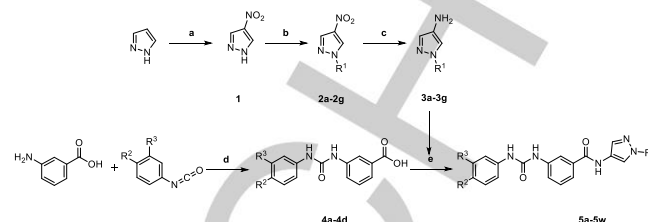
**Figure 1.** (A) The hydrogen bonding mode of the reported molecule with the receptor; (B) The hydrogen bonding mode of sorafenib with the receptor; (C) The construction of new Type II B-Raf kinase inhibitor

## Results and Discussion

## Chemistry

The synthesis of target compounds followed the general pathway outlined in Scheme 1. All of the synthesized compounds are being

reported for the first time and gave satisfactory analytical and spectroscopic data.  $^1\text{H}$ NMR,  $^{13}\text{C}$ NMR, ESI-MS and element analysis spectra were in full accordance with the assigned structures (See in the Supporting Material).



**Scheme 1.** The synthesis routine for target compounds 5a-5w. (a)  $\text{H}_2\text{SO}_4$ ,  $\text{HNO}_3$ ,  $60\text{ }^\circ\text{C}$ , 2 h; (b)  $\text{K}_2\text{CO}_3$ , DMF,  $25\text{ }^\circ\text{C}$ , 16 h; or Iodobenzenes, 8-hydroxyquinoline, CuI,  $\text{K}_2\text{CO}_3$ , DMSO,  $135\text{ }^\circ\text{C}$ , 2 h; (c) 80% hydrazine hydrate, 10% palladium charcoal, ethanol,  $80\text{ }^\circ\text{C}$ , 10 min; (d) THF, rt, 60 h; (e) EDC, HOBT, DMAP, DMF, rt, 18 h.

## Lead compound validation

As demonstrated in Fig. 1, diverse linkers were employed to connect fragment A and B to provide new chemotypes. To these new molecules, consensus docking simulation was performed utilizing type II B-Raf kinase (PDB code: 3IDP, V600E mutant) which has the finest resolution to screen for the best hit. The result suggests the hit compound as shown has the best binding energy, hydrogen bonding with Cys532 in the hinge region, Asp594 in the DFG motif and Glu501 in the  $\alpha\text{C}$  helix (Fig. 2). Van der Waals and other non-covalently interactions also contribute to the binding affinity. Besides, the fragments keep similar interaction modes with their sourced compounds, that is the fragment A remains in the front region and fragment B penetrates into the deep back pocket, fitting into our initial intention.

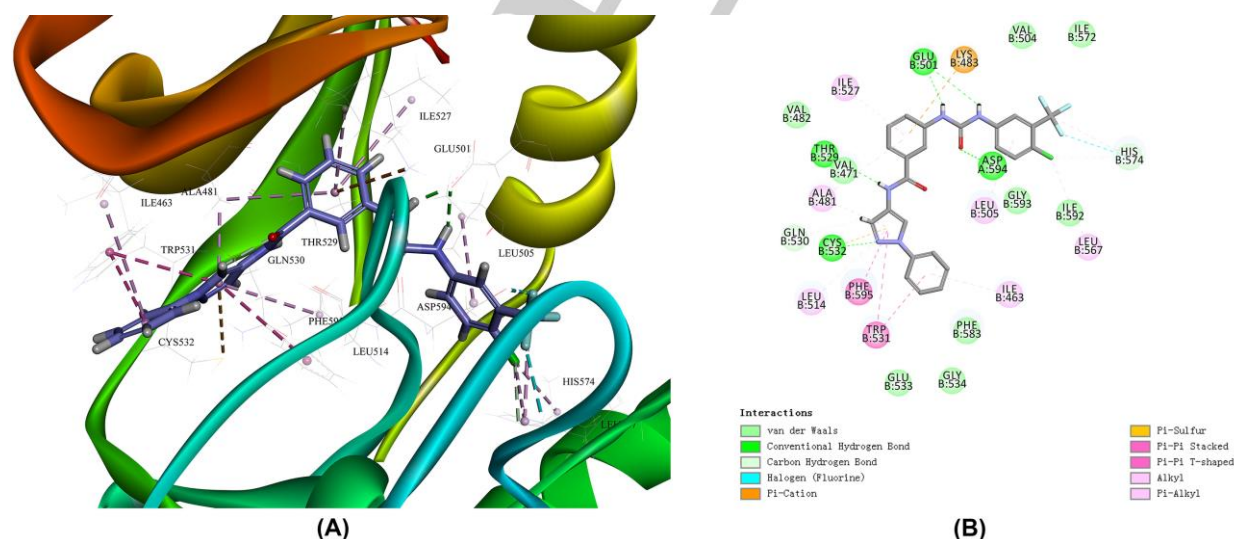


**Figure 2.** The binding mode of hit compound with Type II B-Raf<sup>V600E</sup> kinase in 3D (A) and 2D (B) diagrams. For clarity, only key amino acids are shown.

## Molecular dynamics simulation

A systematic molecular dynamics simulation was carried out to further explore the reliability of the binding model of the hit compound with the receptor and to reveal more details. The

overall RMSD (root mean square deviation) values for both trajectories of ligand and system were counted and exhibited in Fig. 3A. It indicated that the system settled into equilibrium soon after the beginning of the simulation. Both RMSD values kept low

## FULL PAPER

(<0.25 nm and <0.10 nm, respectively) and smooth during the 10 ns dynamics process, hinting at a quite stable state of the binding model. Another characteristic descriptor for the system stability is the Rg (radius of gyration) value for the protein, which is calculated by the distances between centroids of certain molecules and atoms. The fluctuation range of Rg reflects the firmness wobble of protein, and the larger the value is, the relaxer the protein is. In this study, the total Rg and all dimension Rg values were summarized in Fig. 3B. It can be found that the total Rg slightly decreased and remained smooth from 2 ns. Thus the protein kept a stable and compact state during the whole simulation. Also, the final conformation of the complex was overlaid with the initial, and as shown in Fig. 3C, the derivations for both of the proteins and inhibitors were slight. Together these results indicate that the binding system is robust and steady, and can be used as a reliable starting point for further analysis. The heat map for intermolecular hydrogen bonds between the receptor and ligand (Fig 3D) suggests an average number of ~3.98 hydrogen bonds contributed to the binding during the

dynamics simulation. The estimated number of hydrogen bonds in dynamic was in accordance with that gained from the binding result (4 hydrogen bonds). We also calculated the average binding energy for the last 2 ns by MM/PBSA, which was summarized in Fig. 3E. As shown, Van der Waal interaction, electrostatic interaction, polar solvation and non-polar solvation comprised the free binding energy, which summed up to  $-207.409 \pm 18.784$  kJ·mol<sup>-1</sup>, comparable to or even better than some known drugs. The contribution of nearby amino residues for the binding with the ligand was also explored. Important residues were mapped in Fig. 3F, and generally those residues interacting to the ligand (revealed by the docking simulation) contributed higher energy values to the binding. Typically, Glu501, Cys532, and Asp594 which hydrogen bond with the ligand and other residues non-covalently interacting with the ligand provided more energy than other residues, meanwhile some residues went against the binding affinity. The analysis of residue contribution, along with the docking simulation, gives a deeper insight into the further medicinal chemistry optimization.

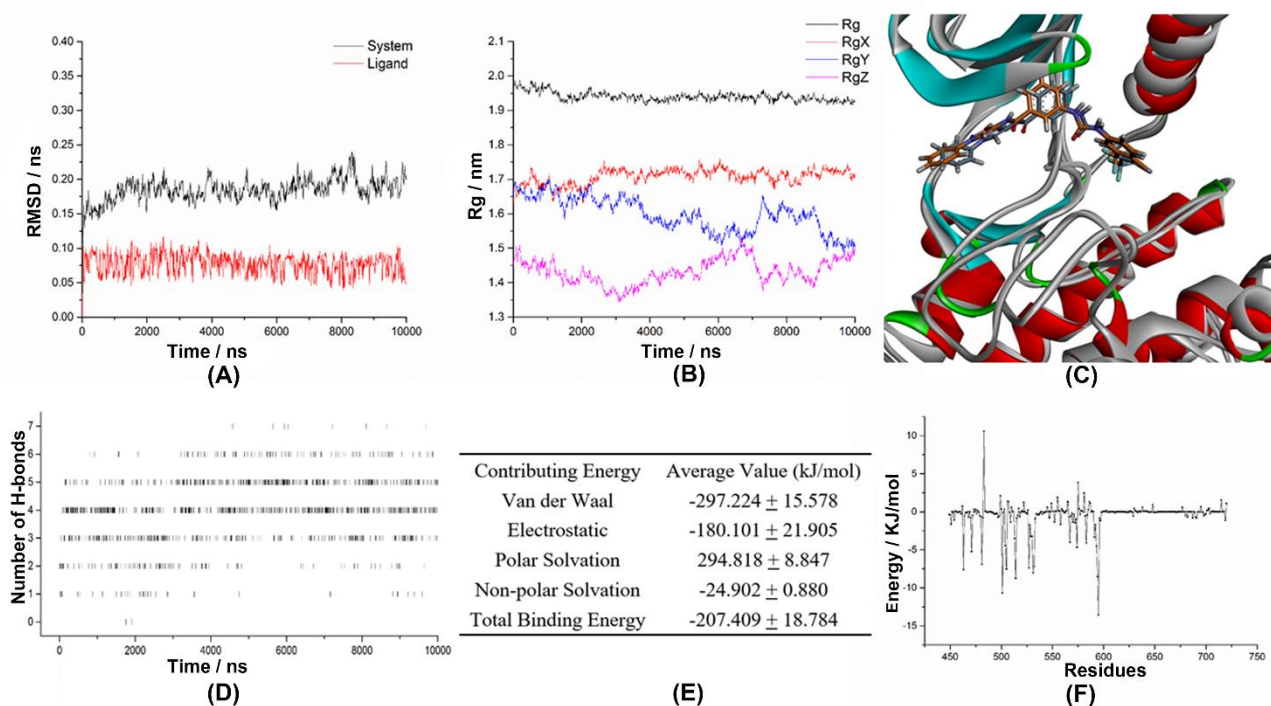


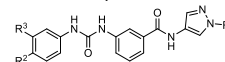
**Figure 3.** (A) The trajectory RMSD values for both system and ligand. (B) The gyration radius values for the receptor. (C) The superimposition of binding systems before (in grey) and after (in color) simulation. (D) The number of H-bonds between ligand and receptor during the simulation. (E) The free binding energy analysis for the binding system. (F) The energy contribution of residues in the binding pocket.

### Scaffold modification and chemical synthesis

After the synergic simulation of virtual docking and molecular dynamics, the lead compound was validated to be capable of binding with B-Raf kinase. Hence we primarily modified its scaffold, mainly focusing on the substitutions on the pyrazole in the front cleft or the phenyl ring in the back pockets. All the derivatives along with their analog sorafenib were evaluated by consensus docking simulation, as listed in Table 1. Many compounds have comparable binding scores to sorafenib, with some bearing even higher scores. Generally, the substitutions on the phenyl ring in the back pocket played a vital role in the binding

affinity. The best substitution (4-chloro-3-(trifluoromethyl)-benzene) contributes more as halogen and other interactions were formed. The binding affinity decreases dramatically when the phenyl has no or a bulky substitution.

**Table 1.** The information of final compounds and their docking scores.



## FULL PAPER

Compound	R <sup>1</sup>	R <sup>2</sup>	R <sup>3</sup>	-Glide gscore					
					<b>5o</b>	-CH <sub>3</sub>		H	9.17
<b>5a</b>	-CH <sub>3</sub>	H	H	9.15	<b>5p</b>	-CH <sub>2</sub> CH <sub>3</sub>		H	8.86
<b>5b</b>	-CH <sub>2</sub> CH <sub>3</sub>	H	H	9.35	<b>5q</b>	-CH <sub>3</sub>	-Cl	-CF <sub>3</sub>	11.18
<b>5c</b>		H	H	11.24	<b>5r</b>	-CH <sub>2</sub> CH <sub>3</sub>	-Cl	-CF <sub>3</sub>	11.26
<b>5d</b>		H	H	8.39	<b>5s</b>		-Cl	-CF <sub>3</sub>	11.82
<b>5e</b>		H	H	8.37	<b>5t</b>		-Cl	-CF <sub>3</sub>	12.04
<b>5f</b>		H	H	8.45	<b>5u</b>		-Cl	-CF <sub>3</sub>	10.56
<b>5g</b>		H	H	9.09	<b>5v</b>		-Cl	-CF <sub>3</sub>	10.97
<b>5h</b>	-CH <sub>3</sub>	-CF <sub>3</sub>	H	10.61	<b>5w</b>		-Cl	-CF <sub>3</sub>	10.61
<b>5i</b>	-CH <sub>2</sub> CH <sub>3</sub>	-CF <sub>3</sub>	H	10.77	<b>sorafenib</b>	-	-	-	11.52
<b>5j</b>		-CF <sub>3</sub>	H	12.02					
<b>5k</b>		-CF <sub>3</sub>	H	9.32					
<b>5l</b>		-CF <sub>3</sub>	H	9.59					
<b>5m</b>		-CF <sub>3</sub>	H	10.68					
<b>5n</b>		-CF <sub>3</sub>	H	10.65					

**Table 2.** The molecular properties of compounds **5a-5w**.

Compound	AlogP	MW	Number of H-acceptor	Number of H-donor	Number of rotatable bonds	Number of aromatic rings	Polar surface area
<b>5a</b>	1.95	335.36	3	3	4	3	0.27
<b>5b</b>	2.30	349.38	3	3	5	3	0.26
<b>5c</b>	3.54	411.45	3	3	6	4	0.22
<b>5d</b>	3.53	397.42	3	3	5	4	0.23
<b>5e</b>	4.02	411.45	3	3	5	4	0.22
<b>5f</b>	3.51	427.45	4	3	6	4	0.24
<b>5g</b>	3.51	427.45	4	3	6	4	0.24
<b>5h</b>	2.89	403.35	3	3	5	3	0.24
<b>5i</b>	3.24	417.38	3	3	6	3	0.23
<b>5j</b>	4.48	479.45	3	3	7	4	0.20
<b>5k</b>	4.47	465.42	3	3	6	4	0.21
<b>5l</b>	4.96	479.45	3	3	6	4	0.20
<b>5m</b>	4.45	495.45	4	3	7	4	0.22
<b>5n</b>	4.45	495.45	4	3	7	4	0.22
<b>5o</b>	4.48	427.46	4	3	6	4	0.20
<b>5p</b>	5.01	441.49	4	3	7	4	0.20
<b>5q</b>	3.56	437.80	3	3	5	3	0.22
<b>5r</b>	3.91	451.82	3	3	6	3	0.22
<b>5s</b>	5.14	513.89	3	3	7	4	0.19
<b>5t</b>	5.14	499.87	3	3	6	4	0.20
<b>5u</b>	5.62	513.89	3	3	6	4	0.19
<b>5v</b>	5.12	529.89	4	3	7	4	0.20
<b>5w</b>	5.12	529.89	4	3	7	4	0.20

We further estimated the drug-likeness property of all the derivatives. As shown in Table 2, all the compounds satisfied most criterions of the "Rules of 5", except the number of rotatable bonds. However, given that many known B-Raf inhibitors also have more rotatable bonds (sorafenib with 6 rotatable bonds and vemurafenib with 7, etc), this rule seems to be less important in this case.

## FULL PAPER

<b>sorafenib</b>	4.17	464.82	4	3	6	3	0.22
<b>vemurafenib</b>	5.68	489.92	4	2	7	4	0.23

**Inhibitory activity on kinases and cancer cells**

With sorafenib and vemurafenib as the reference drugs, all the new compounds were evaluated for the B-Raf<sup>V600E</sup> kinase inhibitory effects. As shown in Table 3, overall the synthesized agents showed moderate to potent inhibitory towards the kinase. Compounds **5v** showed the most prominent inhibitory effect on B-

Raf<sup>V600E</sup> kinase with IC<sub>50</sub> value of 0.035 ± 0.004 μm. Subsequently, the inhibitory activity of **5v** on B-Raf<sup>WT</sup>, C-Raf, p38α, VEGFR2 and JNK1 kinases were further tested (Table 4). The results showed the inhibitory activity of compound **5v** on the other kinases was much lower. In summary, compound **5v** had stronger inhibitory activity and higher selectivity for the B-Raf<sup>V600E</sup> kinase.

**Table 3.** *In vitro* antiproliferative activity and B-Raf<sup>V600E</sup> inhibitory activity of **5a-5w**.

Compound	IC <sub>50</sub> (μm) <sup>[a]</sup>					
	HT29	HCT116	A375	WM1361	B-Raf <sup>V600E</sup>	293T
<b>5a</b>	20.15 ± 1.52	35.57 ± 1.96	16.19 ± 1.03	30.15 ± 1.70	5.82 ± 0.44	> 50
<b>5b</b>	19.75 ± 1.83	34.22 ± 1.52	12.21 ± 1.25	29.35 ± 1.56	6.17 ± 0.52	> 50
<b>5c</b>	12.68 ± 1.20	25.11 ± 1.12	9.24 ± 0.88	18.47 ± 1.62	3.49 ± 0.23	> 50
<b>5d</b>	10.53 ± 0.87	22.26 ± 1.05	8.18 ± 0.69	19.22 ± 1.44	1.56 ± 0.12	> 50
<b>5e</b>	8.82 ± 0.91	20.85 ± 1.39	6.59 ± 0.87	17.80 ± 1.18	2.97 ± 0.19	> 50
<b>5f</b>	10.41 ± 1.03	20.41 ± 2.01	7.54 ± 0.59	16.57 ± 1.05	3.09 ± 0.34	> 50
<b>5g</b>	8.06 ± 0.89	18.18 ± 0.73	5.89 ± 0.85	15.35 ± 1.21	1.23 ± 0.09	> 50
<b>5h</b>	2.55 ± 0.81	8.66 ± 0.95	2.28 ± 0.34	10.45 ± 0.91	0.95 ± 0.11	> 50
<b>5i</b>	3.08 ± 0.29	11.38 ± 1.01	3.21 ± 0.29	12.55 ± 1.06	1.25 ± 0.15	> 50
<b>5j</b>	9.12 ± 0.68	16.87 ± 1.19	8.12 ± 0.92	18.18 ± 1.08	1.64 ± 0.18	> 50
<b>5k</b>	6.01 ± 0.65	13.12 ± 1.04	5.45 ± 0.76	16.68 ± 0.95	1.01 ± 0.13	> 50
<b>5l</b>	4.18 ± 0.54	9.89 ± 0.82	3.85 ± 0.47	15.82 ± 1.27	0.92 ± 0.07	> 50
<b>5m</b>	6.65 ± 0.82	12.81 ± 0.99	4.38 ± 0.62	18.25 ± 1.24	1.21 ± 0.08	> 50
<b>5n</b>	3.15 ± 0.57	9.62 ± 0.87	3.56 ± 0.51	15.86 ± 1.35	0.09 ± 0.01	> 50
<b>5o</b>	19.72 ± 1.53	32.44 ± 1.21	15.11 ± 1.07	29.25 ± 1.75	4.32 ± 0.52	> 50
<b>5p</b>	21.66 ± 1.58	36.35 ± 1.57	16.49 ± 1.12	31.08 ± 1.88	5.11 ± 0.61	> 50
<b>5q</b>	4.65 ± 0.35	19.41 ± 0.99	3.98 ± 0.38	12.54 ± 0.87	0.16 ± 0.02	> 50
<b>5r</b>	5.91 ± 0.56	20.52 ± 1.11	4.12 ± 0.64	17.65 ± 1.15	0.25 ± 0.04	> 50
<b>5s</b>	3.58 ± 0.45	16.58 ± 1.03	3.01 ± 0.42	15.46 ± 0.98	0.21 ± 0.03	> 50
<b>5t</b>	1.06 ± 0.11	9.12 ± 1.84	1.54 ± 0.17	9.88 ± 1.21	0.10 ± 0.01	> 50
<b>5u</b>	0.77 ± 0.09	7.52 ± 0.57	0.65 ± 0.08	8.69 ± 0.92	0.052 ± 0.007	> 50
<b>5v</b>	1.23 ± 0.16	6.88 ± 0.64	0.39 ± 0.04	7.12 ± 1.01	0.035 ± 0.004	> 50
<b>5w</b>	2.38 ± 0.25	11.47 ± 0.96	3.11 ± 0.28	10.23 ± 0.85	0.35 ± 0.05	> 50
<b>vemurafenib</b>	1.56 ± 0.24	18.25 ± 2.65	1.08 ± 0.26	17.34 ± 1.32	0.031 ± 0.008	> 50
<b>sorafenib</b>	9.78 ± 0.86	12.99 ± 1.17	8.36 ± 0.54	10.15 ± 0.98	0.048 ± 0.006	> 50

[a] Data are shown as mean ± SD of three independent experiments.

The compounds were also tested by MTT assay for anti-proliferative activity against two melanoma cancer cell lines, A375 (B-Raf<sup>V600E</sup>) and WM1361 (B-Raf<sup>WT</sup>), along with two colon cancer

cell lines, HT29 (B-Raf<sup>V600E</sup>) and HCT116 (B-Raf<sup>WT</sup>). Besides, human kidney epithelial cell 293T was employed as the non-cancer cell line to evaluate the cytotoxicity of all the compounds,

## FULL PAPER

as summarized in Table 3. A similar inhibitory effect can be observed for the compounds against A375 cell. Toward another B-Raf<sup>V600E</sup> harbored cell line HT29, the inhibitory effects were also significant compared to B-Raf<sup>WT</sup> cell line HCT116. The cytotoxicity values of all tested compounds against 293T were all above 50  $\mu\text{m}$ , indicating a high selectivity over the normal cell lines. Especially, compound **5v** showed the most potent anti-proliferative activity to A375 and HT29 cells expressing B-Raf<sup>V600E</sup> with lower IC<sub>50</sub> values ( $0.39 \pm 0.04 \mu\text{m}$  and  $1.23 \pm 0.16 \mu\text{m}$ ) compared with vemurafenib ( $1.08 \pm 0.26 \mu\text{m}$  and  $1.56 \pm 0.24 \mu\text{m}$ ). In addition, against WM1361 and HCT116 cells expressing B-Raf<sup>WT</sup>, compound **5v** showed a decreased anti-proliferative effect on the contrary. In short, **5v** is a potential B-Raf<sup>V600E</sup> inhibitor and efficiently inhibit the proliferation of tumor cells expressing B-Raf<sup>V600E</sup>.

**Table 4.** Inhibition of kinases activity by compound **5v**.

Kinase	IC <sub>50</sub> ( $\mu\text{m}$ ) <sup>[a]</sup>
B-Raf <sup>V600E</sup>	$0.035 \pm 0.004$
B-Raf <sup>WT</sup>	$0.22 \pm 0.04$
C-Raf	$0.62 \pm 0.08$
p38 $\alpha$	$26.2 \pm 2.12$
VEGFR2	$13.4 \pm 1.87$
JNK1	$10.7 \pm 1.24$

[a] Data are shown as mean  $\pm$  SD of three independent experiments.

### SAR analysis and 3D-QSAR model

Based on the *in vitro* B-Raf<sup>V600E</sup> kinase assay and cellular antiproliferation assay, it could be found that to a certain extent, the potency of the compounds keeps up with their virtual binding affinity. Compounds with an oxydibenzene group (**5o**, **5p**) in the BP region have low potency, for the bulky substitution may hinder the formation of hydrogen bonds between the residues with urea group. Meanwhile, halogen and trifluoromethyl substitutions on the same phenyl improve the potency, compared to those non-substituted (e.g., **5v**>**5m**>**5f**). This result is in accordance with the suggestion by virtual simulation that halogen and trifluoromethyl groups provide additional interactions favoring the binding. As to the investigated groups in the front cleft, substituted phenyl groups tend to be more favorable than alkanes and especially compounds with 4-methoxyl phenyl exhibited better inhibitory activity.

We also established a 3D-QASR model to gain more analysis and have better understanding. All the molecules were converted to the active conformation and attributed with corresponding pIC<sub>50</sub> (mm) values before randomly partitioned into the training set and test set. CHARMM force field and PLS regression were employed in building the model. A scatter plot was obtained with conventional R<sup>2</sup> of 0.9189 (Fig. 4), hinting a high compatibility between the predicted and actual pIC<sub>50</sub> values.

Critical regions (steric or electrostatic) which affect the binding of compounds and enzyme were marked in Fig. 5: compounds were aligned with the iso-surfaces of the 3D-QSAR model coefficients on van der Waals grids (Fig. 5A) and electrostatic potential grids (Fig. 5B). The steric map shows energy grids corresponding to

the favorable (in green) or unfavorable (in yellow) steric effects while information of favorable (in blue) or unfavorable (in red) electrostatic field regions is also given in a contour plot. A good compliance is observed between the model and the actual situation for the tested compounds. Hence, optimized agents may be developed utilizing this model in the future study.

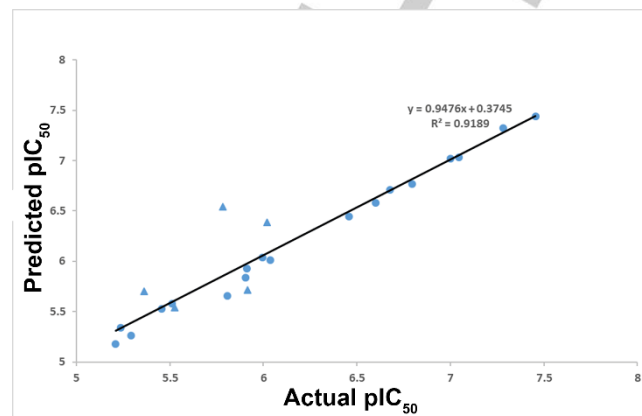


**Figure 4.** Plot of actual vs. predicted pIC<sub>50</sub> of the training set (dots) and test set (triangles).

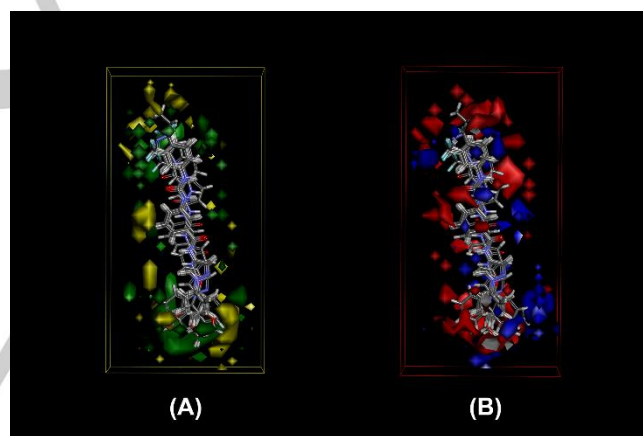


**Figure 5.** (A) 3D QSAR model coefficients on van der Waals grids. Green represents positive coefficients; yellow represents negative coefficients (B) 3D QSAR model coefficients on electrostatic potential grids. Blue represents positive coefficients; red represents negative coefficients.

### Cell apoptosis analysis

To determine whether compound **5v** induced cell apoptosis, an Annexin V/PI double staining assay was conducted. A375 cells were treated with increasing concentrations (0, 2, 4 and 8  $\mu\text{m}$ ) of **5v** or vemurafenib for 24 h, followed by Annexin V/PI double staining and flow cytometric measurement. The increased apoptotic rate was detected after cells being treated with escalating doses of **5v**. As shown in Fig. 6A, the percentages of cell apoptosis 10.22%, 30.3%, 48.5%, 75.5% correspond to the concentration of **5v** 0, 2, 4 and 8  $\mu\text{m}$ , respectively, including both the early and the late apoptotic cells. Clearly, **5v** can cause apoptosis more effectively than vemurafenib. Moreover, an extend time-course apoptosis analysis of A375 cells treated with 4  $\mu\text{m}$  **5v** was carried out. The results indicated that longer treatment periods showed an increase in the percentage of

## FULL PAPER

apoptotic cells (Fig. 6B). Taken together, compound **5v** could induce A375 cells apoptosis in a dose- and time-dependent manner.

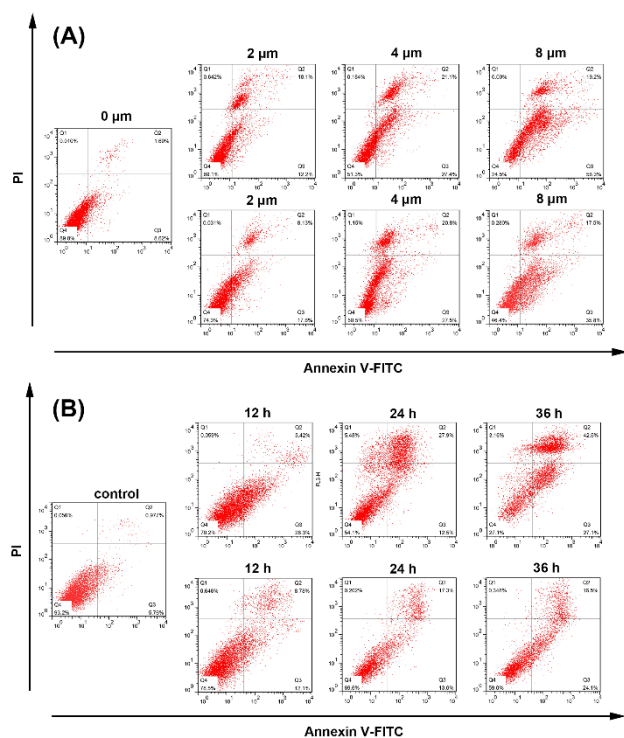


**Figure 6.** (A) A375 cells treated with 0, 2.0, 4.0 and 8.0 μM **5v** and vemurafenib for 24 h were collected and analyzed. (B) A375 cells treated with 4.0 μM **5v** and vemurafenib for 0, 12, 24, 36 h were collected and analyzed. The percentage of early apoptotic cells was shown in the lower right quadrant (Annexin V-FITC positive/PI negative cells), and late apoptotic cells are located in the upper right quadrant (Annexin V-FITC positive/PI positive cells).

### Cell cycle analysis

We further assessed the cell cycle distribution of A375 cells by flow cytometry. A375 cells were treated with compound **5v** at various doses (0, 2, 4, and 8 μM) for 24 h. As illustrated in Fig. 7A, the accumulation of cells in G0/G1 phase increased with increasing drug concentration, and 69.31% of cells were arrested in the G0/G1 phase upon exposure to 4 μM compound **5v** for 24 h. When the concentration of compound **5v** increased to 8 μM, 78.73% of cells were arrested in the G0/G1 phase. Meanwhile, A375 cells were treated with 4 μM compound **5v** at gradient times (0, 12, 24 and 36 h). The accumulation of cells in G0/G1 phase was markedly elevated in a time-dependent manner (with the percentage of 53.11%, 59.42%, 67.85% and 78.42%, Fig. 7B). In summary, **5v** could induce cell cycle arrest in the G0/G1 phase, and the effect was more potent than vemurafenib.

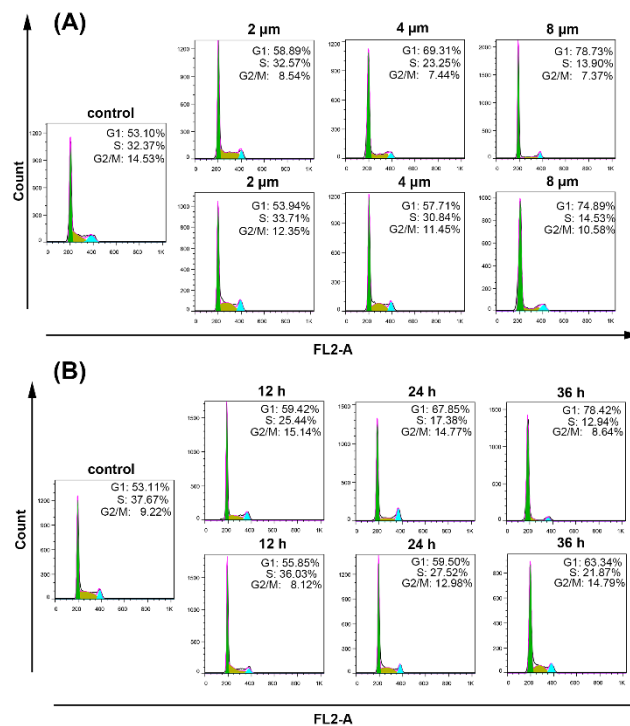


**Figure 7.** (A) A375 cells were treated with 0, 2.0, 4.0 and 8.0 μM **5v** and vemurafenib for 24 h. (B) A375 cells were treated with 4 μM **5v** and vemurafenib for 0, 12, 24, and 36 h. Effect of compound **5v** on the cell-cycle progression of A375 cells was determined by flow cytometry analysis (G0/G1 phase, green; S phase, yellow and G2/M phase, blue).

### Western blot analysis

While the abnormally activated ERK pathway caused by B-Raf<sup>V600E</sup> results in the phosphorylated level of MEK and ERK increased, effective B-Raf<sup>V600E</sup> inhibitors shall block the pathway and down-regulate the expression of pERK and pMEK. The ability of **5v** inhibits ERK and MEK phosphorylation was investigated in A375 cells, with vemurafenib as a positive control drug. As shown in Fig. 8(A) and 8(B), compound **5v** and vemurafenib both reduced the expression of the phosphorylation of ERK and MEK in A375 cells in a dose-dependent manner and had no effect on total expression of ERK and MEK. By comparison, we found that the inhibitory effect of **5v** was more potent than vemurafenib. Subsequently, the abilities of **5v** and vemurafenib inhibiting the phosphorylation of ERK and MEK in WM1361 cells were also evaluated. While the paradoxical effects of vemurafenib at different concentrations were reported, the treatment to WM1361 cells with **5v** showed no significant effect on phosphorylation of ERK and MEK, as shown in Fig. 9.

## FULL PAPER

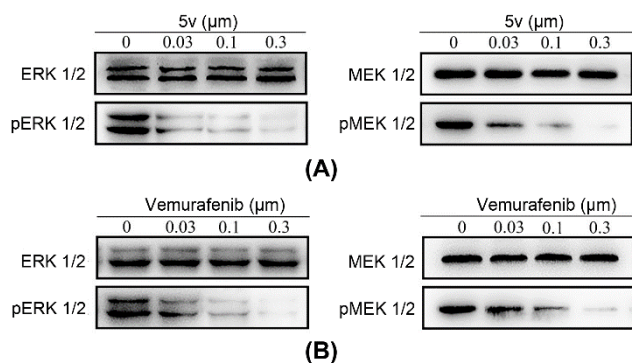


**Figure 8.** (A) **5v** inhibited the phosphorylation of ERK and MEK in A375 melanoma cells bearing B-Raf<sup>V600E</sup> at different doses; (B) Vemurafenib inhibited the phosphorylation of ERK and MEK in A375 melanoma cells bearing B-Raf<sup>V600E</sup> at different doses.

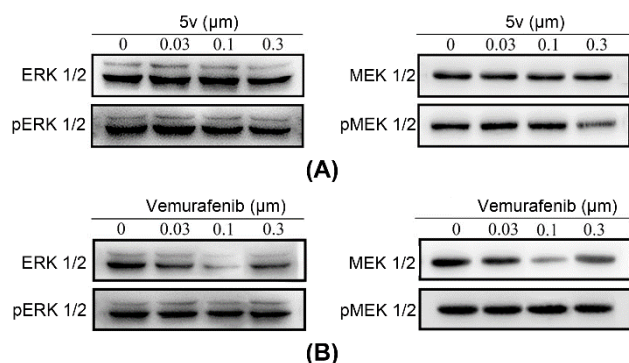


**Figure 9.** (A) **5v** slightly inhibited the phosphorylation of ERK and MEK in WM1361 melanoma cells bearing B-Raf<sup>WT</sup> when dose increased; (B) Vemurafenib paradoxically inhibited the phosphorylation of ERK and MEK in WM1361 melanoma cells bearing B-Raf<sup>WT</sup>.

### Xenografts models

We utilized xenograft models of A375 cells to determine whether compound **5v** inhibited tumor growth *in vivo*. When the tumors began to grow (50–80 mm<sup>3</sup>), the mice were randomly divided into 6 groups (six mice/group) and administrated intraperitoneally with vector, 2.5 mg/kg, 5 mg/kg, 10 mg/kg compound **5v** or 5 mg/kg vemurafenib as a positive control every second day for 15 days. The average tumor volume recorded every other day was shown in Fig. 10A. While the vehicle control group was observed with a rapid development in tumor size, the other groups had distinctly different shapes in the growth curve. At the end of the experiment, tumors were excised and weighed. The average weight of the control group tumors was more than 3-fold to the **5v**-treated mice at the 10 mg/kg dose. When exerted on the same dose of 5 mg/kg, **5v** exhibited equivalent antitumor efficacy in comparison with the positive control drug vemurafenib (Fig. 10B). Briefly, the administration of **5v** inhibited tumor growth in a dose-dependent manner. Meanwhile, **5v** did not show a significant effect on the body weight (Fig. 10C), as well as the weight of the liver or spleen (Fig. 10D). It can be concluded that the administration of **5v** up to 10 mg/kg didn't cause weight loss, liver harm or spleen swelling, hinting a considerable safety *in vivo*. Together, these *in vivo* data indicate that **5v** exhibits excellent antitumor ability and may

become a promising lead compound for the development of novel antitumor drugs.

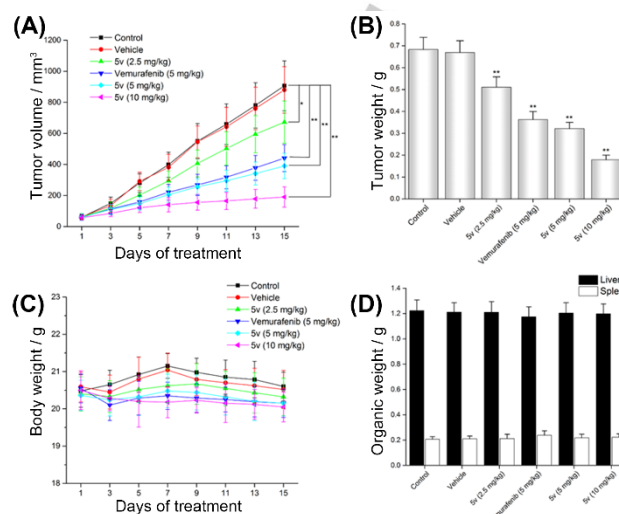


**Figure 10.** (A) Tumor volumes. A375 cells were injected subcutaneously into the right flank of nude mice. When the treatment began, the tumor volumes were monitored and recorded every two days; (B) Tumor weight on day 15 of treatment; (C) Body weight. When the treatment began, the body weight was monitored and recorded every two days; (D) Weight of liver and spleen on day 15. Data are shown as mean  $\pm$  SD. \* $P < 0.05$ , \*\* $P < 0.01$ .

### Conclusions

In light of the drawbacks of the known B-Raf inhibitors, great efforts have been made to optimize the existing agents and to explore new chemical space. On the whole, the massive studies both depicting the biological mechanisms of Raf kinase and revealing the interaction mode between inhibitors and Raf kinase have pointed out the direction for better-performance agents. Yet attempts to do so still need to take many factors into consideration, such as breaking the paradoxical effects in kinases. Our previous and current efforts mainly focused on the recombination of high-efficient fragments from different sources into a new molecule. The synergic simulation was carried out in this work: while the consensus docking by various applications eliminated the deviations between algorithms to a certain extent, the molecular dynamics as a validated post-docking tool further tested the credibility of the binding model. The analyses of MD were in high accordance with the result of docking simulation, and it also provided more details which may benefit future study. The molecular properties were investigated to evaluate the drug-likeness of the new compounds. Overall, the analyses gave interesting results and thereby we synthesized all the compounds. By *in vitro* assays of anti-proliferation and kinases inhibition, the best compound **5v** was selected and underwent further bioassays to depict its pharmacological profile and give SAR suggestions. Nude mice xenograft models were also established to demonstrate the *in vivo* performance of **5v**. All results together suggest we have identified a new series of B-Raf<sup>V600E</sup> inhibitors and we hope such efforts shall provide new insight into the related studies.

## FULL PAPER

## Experimental Section

## Materials

All chemicals (reagent grade) used were purchased from Nanjing Chemical Reagent Co. Ltd. (Nanjing, China). Vemurafenib was purchased from Sigma-Aldrich (St. Louis, MO). All the  $^1\text{H}$  NMR spectra were recorded on a Bruker DPX 600 model spectrometer in  $\text{DMSO}-d_6$ , and chemical shifts ( $\delta$ ) are reported as parts per million (ppm). ESI-MS spectra were recorded by a Mariner System 5304 Mass spectrometer. Elemental analyses were performed on a CHN-O-Rapid instrument and were within 0.4% of the theoretical values. Melting points were determined on an XT4 MP apparatus (Taikhe Corp, Beijing, China). Purity of compounds were tested by HPLC (purity > 95%). Thin layer chromatography (TLC) was performed on silica gel plates (Silica Gel 60 GF254) and visualized in UV light (254 nm and 365 nm). Column chromatography was performed using silica gel (200 - 300 mesh) and eluting with ethyl acetate and petroleum ether (bp. 30 - 60 °C). A375 cells were kindly provided by Stem Cell Bank, Chinese Academy of Sciences. The other cell lines (WM1361, HT29 and HCT116) were preserved in the State Key Laboratory of Pharmaceutical Biotechnology of Nanjing University. The AnnexinV-FITC cell apoptosis assay kit was purchased from Vazyme Biotechco., Ltd (Nanjing, China). The Raf kinases were purchased from Invitrogen (US). All antibodies were obtained from WanleiBio (Shenyang, China). The *balb/c* nude mice (female, 6 - 8 weeks, 20 - 21 g) were purchased from Nanjing University Animal Center (Nanjing, China).

## Chemistry

## Synthesis of compound 1

Pyrazole (2 g, 29.4 mmol) was dissolved in concentrated sulfuric acid (6 mL). Afterward the solution was heated to 60 °C, before the dropwise addition of nitric acid (1.2 mL). The reaction was stirred for 2 h and poured into ice water. A white precipitate (**1**) formed which was filtered and washed with water. The filtrate was neutralized using sodium carbonate and extracted with ethyl acetate (3 × 20 mL). The combined organic phases were washed by brine solution, dried over sodium sulfate and concentrated *in vacuo* to give the rest product **1**.

## Synthesis of compounds 2a-2g

A mixture of alkane or aryl iodide (6.82 mmol), **1** (0.7 g, 6.2 mmol), 8-hydroxyquinoline (0.09 g, 0.62 mmol), cuprous iodide (0.18 g, 0.62 mmol) and potassium carbonate (1.73 g, 12.4 mmol) in DMSO (10 mL) was heated at 135 °C overnight. After cooling to rt, the reaction mixture was diluted with 20 mL of water and extracted with ethyl acetate. The organic layer was washed with aqueous saturated sodium bicarbonate, dried by sodium sulfate, filtered and concentrated *in vacuo*. Purification by flash chromatography (petroleum ether : ethyl acetate = 6 : 1) gave the desired products **2a-2g**.

## Synthesis of compounds 3a-3g

To a solution of **2a-2g** (4.5 mmol) in 4 mL ethanol was added 80% hydrazine hydrate (2 mL) and 10% palladium charcoal (0.08 g). The reaction was refluxed for 10 min and filtered by celite *in vacuo*. The filtrate was dried by sodium sulfate and concentrated to afford compounds **3a-3g**, which were used without further purification.

## Synthesis of compounds 4a-4d

To a solution of 3-aminobenzoic acid (2 mmol, 0.27 g) in 15 mL THF was dropwise added phenyl isocyanates (2 mmol). The mixture was stirred for 60 h at rt and filtered. The solid was washed with cold dichloromethane and ethyl acetate (3 × 5 mL) to give the pure compounds **4a-4d**.

## Synthesis of compounds 5a-5w

EDC (1.5 mmol, 0.28 g) was added in one portion to a mixture of **4a-4b** (1.5 mmol) and HOBt (1.5 mmol, 0.2 g) in DMF (4.00 mL) at 25 °C for 30 min. Then DMAP (1.5 mmol, 0.19 g), **3a-3g** (1.5 mmol), and  $\text{Et}_3\text{N}$  (1 mL) were added and the reaction mixture was stirred overnight. The resulting mixture was poured into water and was extracted with ethyl acetate. Purification by flash chromatography (petroleum ether : ethyl acetate = 6 : 1) gave the desired products **5a-5w**.

## Virtual simulation

The consensus docking simulation and graphics processing work were carried out following the procedure described previously.<sup>[15]</sup> Molecular dynamics simulations were carried out using the GROMACS package version 5.1.2 with GPU-accelerating supported. The parameter setting and operating procedure can be seen in previous reports.<sup>[16]</sup> A ligand-based 3D-QSAR model was established by the QSAR module of DS 3.5, following the same protocol reported in the previous work.<sup>[17]</sup>

## Biological assays

All the biological assays were carried out following the protocols from product manufacturers or reference literature.<sup>[14-16, 18]</sup> Animal welfare and experimental procedures were followed in accordance with the Guide for Care and Use of Laboratory Animals (National Institutes of Health, the United States) and the related ethical regulations of Nanjing University.

## Statistical analysis

All assays, with established cell lines, were repeated three times. All data are expressed as mean  $\pm$  SD. The statistical analysis was performed by the Student's *t*-test, and if appropriate, by a one-way ANOVA test, using the statistical software OriginPro 2015.

## Acknowledgements

The work was financed by the Public Science and Technology Research Funds Projects of Ocean (No. 201505023), the International Postdoctoral Exchange Fellowship Program 2017 (No. 20170090) and Nanjing University Undergraduate Innovation Program and the National Natural Science Foundation of China (No. J1210026).

**Keywords:** B-Raf inhibitors; molecular optimization; *in silico*; rational design; mice xenograft

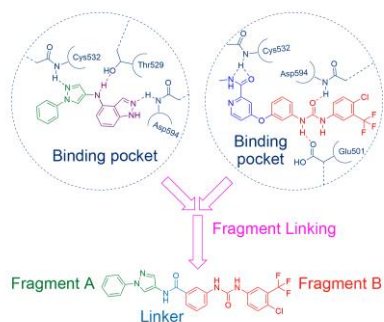
## References:

- [1] M. J. Garnett, R. Marais, *Cancer Cell* **2004**, *6*, 313-319.
- [2] a) C. Zhang, W. Spevak, Y. Zhang, E. A. Burton, Y. Ma, G. Habets, J. Zhang, J. Lin, T. Ewing, B. Matusow, *Nature* **2015**, *526*, 583-586; b) A. Munshi, R. Ramesh, *Genes & Cancer* **2013**, *4*, 401-408.
- [3] a) M. Holderfield, M. M. Deuker, F. McCormick, M. McMahon, *Nature Reviews Cancer* **2014**, *14*, 455-467; b) M. Xing, A. S. Alzahrani, K. A. Carson, D. Viola, R. Elisei, B. Bendlova, L. Yip, C. Mian, F. Vianello, R. M. Tuttle, *Jama* **2013**, *309*, 1493-1501; c) M. Xing, A. S. Alzahrani, K. A. Carson, Y. K. Shong, T. Y. Kim, D. Viola, R. Elisei, B. Bendlová, L. Yip, C. Mian, *Journal of Clinical Oncology* **2014**, *33*, 42-50.
- [4] a) D. M. Hyman, I. Puzanov, V. Subbiah, J. E. Faris, I. Chau, J.-Y. Blay, J. Wolf, N. S. Rajje, E. L. Diamond, A. Hollebecque, *New England Journal of Medicine* **2015**, *373*, 726-736; b) M. S. Brose, C. M. Nutting, B. Jarzab, R. Elisei, S. Siena, L. Bastholt, C. de la Fouchardiere, F. Pacini, R. Paschke, Y. K. Shong, *The Lancet* **2014**, *384*, 319-328.

## FULL PAPER

- [5] M. Holderfield, T. Nagel, D. Stuart, *British Journal of Cancer* **2014**, *111*, 640-645.
- [6] C. W. Murray, D. C. Rees, *Angewandte Chemie International Edition* **2016**, *55*, 488-492.
- [7] a) O. Klein, A. Ribas, B. Chmielowski, G. Walker, A. Clements, G. V. Long, R. F. Kefford, *Journal of Clinical Oncology* **2013**, *31*, e215-e217; b) C. Bailleux, G. Robert, C. Ginet, D. Re, A. Thyss, I. Sudaka, I. Peyrottes, P. Hofman, P. Auberger, F. Peyrade, *Oncoscience* **2015**, *2*, 44.
- [8] a) Z. Karoulia, E. Gavathiotis, P. I. Poulikakos, *Nature Reviews Cancer* **2017**; b) S. Wilhelm, C. Carter, M. Lynch, T. Lowinger, J. Dumas, R. A. Smith, B. Schwartz, R. Simantov, S. Kelley, *Nature Reviews Drug Discovery* **2006**, *5*, 835-844.
- [9] a) T. E. Williams, S. Subramanian, J. Verhagen, C. M. McBride, A. Costales, L. Sung, W. Antonios-McCrea, M. McKenna, A. K. Louie, S. Ramurthy, *ACS Medicinal Chemistry Letters* **2015**, *6*, 961-965; b) P. Lito, N. Rosen, D. B. Solit, *Nature Medicine* **2013**, *19*, 1401-1409; c) W. Fiskus, N. Mitsiades, *Annual Review of Medicine* **2016**, *67*, 29-43; d) J. Zhang, B. Lu, D. Liu, R. Shen, Y. Yan, L. Yang, M. Zhang, L. Zhang, G. Cao, H. Cao, *Cancer Biology & Therapy* **2016**, *17*, 199-207.
- [10] D. K. Treiber, N. P. Shah, *Chemistry & Biology* **2013**, *20*, 745-746.
- [11] O. P. van Linden, A. J. Kooistra, R. Leurs, I. J. de Esch, C. de Graaf, *Journal of Medicinal Chemistry* **2013**, *57*, 249-277.
- [12] a) S. Wenglowky, D. Moreno, E. R. Laird, S. L. Gloor, L. Ren, T. Risom, J. Rudolph, H. L. Sturgis, W. C. Voegtli, *Bioorganic & Medicinal Chemistry Letters* **2012**, *22*, 6237-6241; b) S. Wenglowky, L. Ren, K. A. Ahrendt, E. R. Laird, I. Aliagas, B. Alick, A. J. Buckmelter, E. F. Choo, V. Dinkel, B. Feng, *ACS Medicinal Chemistry Letters* **2011**, *2*, 342-347.
- [13] G. Verkhivker, *Molecular BioSystems* **2016**, *12*, 3146-3165.
- [14] P. F. Wang, H. Y. Qiu, Z. F. Wang, Y. J. Zhang, Z. C. Wang, D. D. Li, H. L. Zhu, *Biochemical Pharmacology* **2017**, *132*, 63-76.
- [15] H. Y. Qiu, P. F. Wang, Z. Li, J. T. Ma, X. M. Wang, Y. H. Yang, H. L. Zhu, *Pharmacological Research* **2016**, *104*, 86-96.
- [16] a) H. Y. Qiu, X. Zhu, Y. L. Luo, H. Y. Lin, C. Y. Tang, J. L. Qi, Y. J. Pang, R. W. Yang, G. H. Lu, X. M. Wang, Y. H. Yang, *Scientific Reports* **2017**, *7*, 2863; b) H.-Y. Qiu, J.-Y. Fu, M.-K. Yang, H.-W. Han, P.-F. Wang, Y.-H. Zhang, H.-Y. Lin, C.-Y. Tang, J.-L. Qi, R.-W. Yang, *Biochemical Pharmacology* **2017**, *146*, 74-86.
- [17] P. F. Wang, H. Y. Qiu, S. K. Baloch, H. B. Gong, Z. C. Wang, H. L. Zhu, *Chemical Biology & Drug Design* **2015**, *86*, 1405-1410.
- [18] P. F. Wang, Y. J. Zhang, D. Wang, H. M. Hu, Z. C. Wang, C. Xu, H. Y. Qiu, H. L. Zhu, *Bioorganic & Medicinal Chemistry* **2018**, *26*, 2372-2380.

## FULL PAPER



Based on our previously reported B-Raf inhibitors and known drugs, a new series of type II B-Raf inhibitors were designed by fragment linking strategy. The new compounds were validated by synergic simulations, acquired by synthesis and profiled by *in vitro* and *in vivo* pharmacological assays. Several agents showed excellent performance which worth further study in the future research.